Neutron Resonance Scattering Shows Specific Binding of Plutonium to the Calcium-Binding Sites of the Protein Calmodulin and Yields Precise Distance Information

P. A. Seeger, S. E. Rokop, P. D. Palmer, S. J. Henderson,[†] D. E. Hobart,[‡] and J. Trewhella*

Contribution from the Chemical Science and Technology Division and Manuel Lujan Jr. Neutron Scattering Center, Mail Stop G758, Los Alamos National Laboratory, Los Alamos, New Mexico 87545

Abstract: We have successfully substituted $^{240}Pu^{3+}$ for Ca^{2+} in the calcium-binding protein calmodulin and used neutron resonance scattering from the bound ^{240}Pu to demonstrate that the Pu binds specifically to the Ca^{2+} sites and also to measure the distance between the ion binding sites within individual domains of the protein. ^{240}Pu has a strong nuclear resonance at 0.278 Å, and at this wavelength the coherent scattering from ^{240}Pu is >1000 times that of any other nucleus present in a protein. The ionic radius of Pu^{3+} is very similar to that of Ca^{2+}, and hence we chose this species to substitute for Ca^{2+} in the protein. We identified solution conditions that stablize Pu^{3+} in solution at near neutral pH for 6−7 h in order to form the Pu/calmodulin complex under conditions favorable for both complex formation and maintaining the structural integrity of the protein. We collected small-angle neutron scattering data from solutions of $4(^{240}Pu^{3+})$·calmodulin, which contain periodic terms that are directly related to the distances between the Ca^{2+}-binding sites. The shorter Pu−Pu distance, *i.e.*, the average distance between the two sites within each globular domain of calmodulin, is found to be 11.8 ± 0.4 Å, in excellent agreement with the value of 11.7 Å from crystallographic determinations. This is the first use of neutron resonance scattering as a structural probe in a protein.

Introduction

Ca^{2+} is widely used in nature as a messenger to transmit signals by reversibly binding to specific receptor proteins and triggering conformational transitions that in turn result in activation of specific biochemical pathways. Calmodulin (CaM) is the major intracellular receptor for Ca^{2+} in eukaryotic cells and is responsible for the regulation of a diverse array of target enzymes (reviewed in refs 1 and 2). CaM is a relatively small protein (16700 Da, 148 residues), and its structure shows an unusual dumbbell shape with two globular domains connected by a solvent-exposed α-helix of 7−8 turns.[3] Each of the globular domains contains two structurally similar Ca^{2+}-binding sites having a helix−loop−helix structural motif,[4] with the loop regions each presenting seven oxygen atoms (six from the protein and one from a water molecule) in a pentagonal-byramidal geometry to bind a single Ca^{2+} with a mean oxygen−calcium distance of approximately 2.4 Å (reviewed in ref 5). Ca^{2+} binding in these loops results in an "opening" of the globular domains, via a hinge defined within the loop regions,

and exposure of hydrophobic amino acid side chains that play a key role in target enzyme binding. Earlier small-angle scattering studies by us were interpreted as indicating that the globular domains of CaM were on average closer together in solution than in the crystal structure, probably through flexibility in the interconnecting helix region.[6] While initially a point of disagreement, this conclusion is now widely accepted in the light of more recent data from NMR[7,8] and crystallography,[9,10] as well as neutron small-angle solution scattering studies[11,12] on CaM complexed with peptides corresponding to its binding domains in various target enzymes. These studies show that CaM collapses around the helix-forming peptides via the conformational flexibility available in the central helix, which would also facilitate CaM binding to the different stereochemical surfaces presented by different target enzymes.

Neutron-scattering techniques are extremely useful for studying structure and dynamics in condensed matter, including biological systems. Neutron scattering is a quantum mechanical process that depends upon the properties of the compound nucleus that forms between an incoming neutron and a nucleus

* To whom correspondance should be addressed.

[†] Present address: Chemical Engineering and Materials Sciences, University of Oklahoma, Norman, OK 73019.

[‡] Present address: RE/Spec Inc., Albuquerque, NM, and Glenn T. Seaborg Institute of Transactinide Science, Lawrence Livermore Laboratory, Livermore, CA 94551.

[⊗] Abstract published in *Advance ACS Abstracts,* May 15, 1997.

(1) Means, A. R.; VanBerkum, M. F. A.; Bagchi, I.; Lu, K. P.; Rasmussen, C. D. *Pharm. Ther.* **1991**, *50*, 255−270.

(2) O'Neil, K. T.; Degrado, W. F. *Trends Biochem. Sci.* **1990**, *15*, 59−64.

(3) Babu, Y. S.; Sack, J. S.; Greenhough, T. G.; Bugg, C. E.; Means, A. R.; Cook, W. J. *Nature* **1985**, *315*, 37−40.

(4) Kretsinger, R. H.; Moncrief, N. D.; Goodman, M.; Czelusniak, J. *The Calcium Channel: Structure, Function and Implications*; Morad, Naylor, Kazda, and Schramm, Eds.; Springer-Verlag: Berlin, 1988; pp 16−35.

(5) Strynadka, N. C. J.; James, M. N. G. *Annu. Rev. Biochem.* **1989**, *58*, 951−958.

(6) Heidorn, D. B.; Trewhella, J. *Biochemistry* **1988**, *27*, 909−915.

(7) Ikura, M.; Clore, G. M.; Gronenborn, A. M.; Zhu, G.; Klee, C. B.; Bax, A. *Science* **1992**, *256*, 632−638.

(8) Barbato, G.; Ikura, M.; Kay, L. E.; Pastor, R. W.; Bax, A. *Biochemistry* **1992**, *31*, 5269−5278.

(9) Meador, W. E.; Means, A. R.; Quiocho, F. A. *Science* **1992**, *257*, 1251−1255.

(10) Meador, W. E.; Means, A. R.; Quiocho, F. A. *Science* **1993**, *262*, 1718−1721.

(11) Heidorn, D. B.; Seeger, P. A.; Rokop, S. E.; Blumenthal, D. K.; Means, A.R.; Crespi, H.; Trewhella, J. *Biochemistry* **1989**, *28*, 6757−6764.

(12) Trewhella, J.; Blumenthal, D. K.; Rokop, S. E.; Seeger, P. A. *Biochemistry* **1990**, *29*, 9316−9324.

(13) Mughabghab, S. F. *Neutron Scattering Cross Sections: Neutron Resonance Parameters and Thermal Cross Sections*; Academic Press: London, 1984; Vol. 1, Parts A and B.

(14) Lynn, J. E.; Seeger, P. A. *At. Data Nucl. Data Tables* **1990**, *44*, 191−207.

in a sample. As a result, neutron-scattering amplitudes vary irregularly with atomic number (in contrast to X-ray scattering factors that increase linearly with the number of electrons), isotopes of the same element can have very different neutron-scattering properties, and there are strong wavelength-dependent resonance effects. The large differences in neutron-scattering properties between the isotopes of hydrogen (^{1}H and ^{2}H) have been taken advantage of for studies of biological molecules and complexes over the past several decades. Modern accelerator-based spallation neutron sources have opened up the potential for applications of neutron resonance scattering, since they provide pulses of neutrons containing a wide spectrum of wavelengths and time-of-flight methods can be readily used to select the neutrons with the desired wavelength. To date, however, it has been difficult to use neutron resonance scattering as a structural probe due largely to the low neutron fluxes at the wavelengths of interest. There are many nuclei with resonances below ~2 eV, but if we include only those whose coherent scattering is at least 1% of the total cross section, then the list is limited to 11 isotopes: soft metals ^{113}Cd and ^{115}In, rare earths ^{149}Sm, ^{151}Eu, ^{157}Gd, ^{163}Dy, ^{168}Yb, and ^{177}Hf, noble metal ^{193}Ir, and actinides ^{230}Th and ^{240}Pu.[13,14] A number of the resonant nuclei have properties that are similar to those of biologically relevant metals. In particular, ^{240}Pu^{3+} is a positively charged ion with a similar ionic radius as Ca^{2+}, and a good candidate for binding with high affinity to Ca^{2+} sites in proteins. The differences in charge-to-radius ratio between Ca^{2+} and Pu^{3+} would, however, be expected to result in differences in the dynamics of the reversible ion binding, and possibly in the ion-dependent structural transitions that are critical to the normal function of proteins like CaM. Disruption of biochemical regulation by metals via such mechanisms has been discussed;[15,16] however, in the case of Pu, there have been no structural studies to date demonstrating binding to specific sites in a protein.

The neutron resonance scattering experiments we report here were motivated by the desire to see if the technique could work as a structural tool, in particular for proteins in solution, and to learn something of the specificity of binding of Pu to Ca^{2+} regulatory proteins. In proposing an experiment involving resonant scattering from ^{240}Pu substituted for calcium in a biological molecule, it is necessary to address questions of physics (suitability of the resonant scatterer), chemistry (dissolving the atoms in the needed ionization state in an appropriate medium), and biochemistry (binding the substituted atoms at the relevant sites).

Experimental Methods and Results

Physics of Resonant Scattering. Resonant neutron scattering is analogous to anomalous X-ray scattering in that it is sensitive to rapid variations of the interaction probability of a specific atomic species as a function of wavelength. To be useful in resonant scattering, the nuclear resonance must be at a low enough energy (long enough wavelength) to sample appropriate distance scales, must be relatively narrow so that variations are rapid, and must have a strong component of coherent scattering. Of all available nuclei, the neutron resonance at 1.057 eV in ^{240}Pu meets these physics criteria best. Parameters of this resonance have been fitted to existing nuclear data by using a generalized single-level formalism.[17] As shown in Figure 1,

(15) Cox, J. L.; Harrison, S. D. *Biochem. Biophys. Res. Commun.* **1983**, *115*, 106−111.

(16) Pounds, J. G.; Rosen, J. F. *Toxicol. Appl. Pharmacol.* **1988**, *94*, 331−341.

(17) Lynn, J. E. personal communication of the fitted parameters of the ^{240}Pu resonance in the formalism of ref 14.
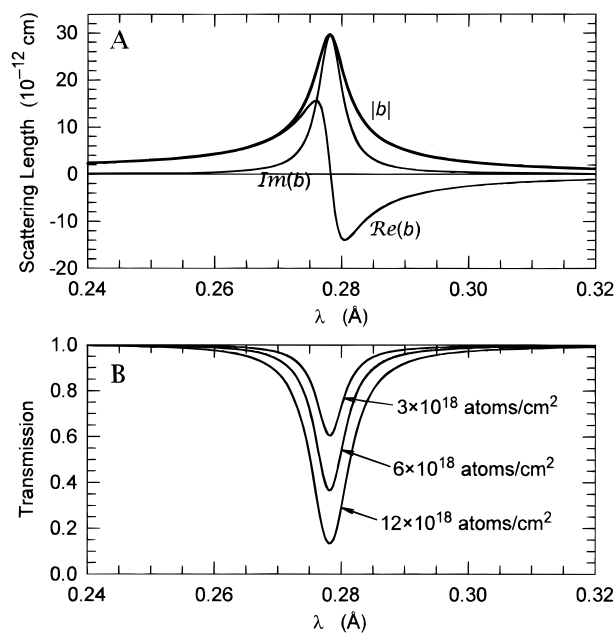

Figure 1. (A) Coherent neutron-scattering length (complex value) near the 1.057-eV resonance of ^{240}Pu. (B) Neutron transmission at the resonance, for various area densities.

this allows a precise computation of the wavelength dependence of both the complex coherent scattering amplitude (which leads to small-angle scattering) and the total cross section (which is essential in correcting for the transmission of the sample in the neighborhood of the resonance). The wavelength at the peak of the resonance is 0.278 Å. Although this is much shorter than the wavelengths usually used for small-angle scattering, and hence will limit the ability to measure small momentum transfer, neutrons of this wavelength are available and well resolved at a pulsed spallation source such as the Manuel Lujan Jr. Neutron Scattering Center (MLNSC) at the Los Alamos Neutron Science Center (LANSCE). Small-angle neutron scattering is determined by coherent interference of all pairs of nuclei in the sample. If a neutron of wavelength λ (velocity $v = h/M_n\lambda$, where h is Plank's constant and M_n is the neutron mass) scatters at an angle of 2θ, then the magnitude of its momentum change (in units of $h/2\pi$) is

$$Q = 4\pi(\sin\theta)/\lambda \qquad (1)$$

and the direction of the **Q** vector is at an angle $(\pi/2 + \theta)$ from the initial velocity. The scattering amplitudes must be summed with a phase factor depending on wavelength and angle, so that the total amplitude of the scattered wave[18] is

$$A(\mathbf{Q}) = \sum b_k \exp(-i\mathbf{Q}\cdot\mathbf{r}_k) \qquad (2)$$

where $\mathbf{r}_k$ is the vector from an arbitrary origin to atom k which has (complex) scattering length b_k. The observable scattering intensity is the square of this amplitude:

$$I(\mathbf{Q}) = A^*(\mathbf{Q})\,A(\mathbf{Q}) = \sum\sum b^*_k\, b_j \exp(-i\mathbf{Q}\cdot\mathbf{r}_{jk})$$
$$= \sum\sum b^*_k\, b_j[\cos(\mathbf{Q}\cdot\mathbf{r}_{jk}) - i\sin(\mathbf{Q}\cdot\mathbf{r}_{jk})] \quad (3)$$

where $\mathbf{r}_{jk}$ is the vector from atom j to atom k. In solution, assuming nonaligned particles, all orientations of $\mathbf{r}_{jk}$ are equally

(18) Guinier, A.; Fournet, G. *Small-Angle Scattering of X-Rays*; John Wiley: New York, 1955; pp 5−8.

probable. In particular the sine term in eq 3 is odd and will vanish when averaged. Also, in the double sum over j and k the odd (imaginary) terms in the coefficient of the even cosine will cancel. The result of spherical averaging is

$$I(Q) = \sum_k \sum_j \mathrm{Re}(b^*_k\, b_j)\, \sin(Qr_{jk})/Qr_{jk} \qquad (4)$$

This is essentially the X-ray scattering equation of Debye,[19] modified to include complex neutron scattering lengths.

For small-angle scattering, the scattering-length densities are generally averaged over larger volumes of space (unlike high-resolution crystal diffraction). In the simple case of a solution of molecules of uniform composition and density in a uniform solvent, the scattering depends on the difference between the average scattering-length density within the molecule and that of the solvent. In the case of resonant scattering, however, the scattering length for the resonant species is so much greater than that of any other atom in the system that we use eq 4 explicitly for all atoms of the resonant species and treat everything else with an average (real) scattering-length density ρ. Using subscript "*r*" to represent resonant scattering and "*0*" for nonresonant, we can express $I(Q,\lambda)$ in terms of nonresonant, interference, and resonant form factors:

$$I(Q,\lambda) = \rho^2 F_{00}(Q) + \mathrm{Re}\{b(\lambda)\}\rho F_{0r}(Q) + |b(\lambda)|^2 F_{rr}(Q) \quad (5)$$

The known and distinctive wavelength dependencies (Figure 1) will allow the form factor $F_{rr}(Q)$ to be extracted. From eq 4, including only terms jk for the resonant species,

$$F_{rr}(Q) = \sum \sum \sin(Qr_{jk})/Qr_{jk} \qquad (6)$$

and information about the interatomic distances r_{jk} of the resonant species can be obtained.

Preparation of Pu^{3+}. Preparation of Pu^{3+} began with isotopically enriched ^{240}PuO$_2$ which was dissolved by heating in concentrated HClO$_4$ with a few drops of 5% hydrofluoric acid. The Pu in solution was oxidized to PuO$_2{}^{2+}$ with fuming HClO$_4$. Hydrazine dihydrochloride was added to reduce the PuO$_2{}^{2+}$ to Pu^{3+}, and NaNO$_2$ was added to oxidize the Pu^{3+} to Pu^{4+}. The Pu^{4+} solution was then purified with an anion exchange column. Pu^{4+} was eluted with 0.5 M HCl and stored as a stock solution. An aliquot of this stock solution was used for addition to CaM solutions. The acid content was reduced further by again loading the Pu^{4+} on an anion exchange column and eluting with 0.25 M HCl. The Pu^{4+} in 0.2 M HCl was reduced to Pu^{3+} in a standard three-electrode electrochemical cell; the working electrode of the cell was a Pt screen, the counter electrode was a Pt wire separated from the experimental solution with a Vicor frit, and the reference electrode was a saturated calomel.[20] After all the Pu was reduced to Pu^{3+}, a strong reducing potential was applied in order to drive off H$^+$ at the Pt screen electrode. This further reduced the acid content of the solution. Solid Na$_2$CO$_3$ was then added to bring the pH to $\sim$4.0. The solution was centrifuged to remove any solid Na$_2$CO$_3$ or Pu^{4+} colloid. The purity of the Pu^{3+} in the supernatant was assessed by spectrophotometry. Figure 2 shows the characteristic absorption spectra for Pu^{4+} and Pu^{3+}. Concentrations of Pu^{3+} were determined from the absorbance at 600 nm.

Protein Preparation. Protein samples were prepared with bacterially synthesized CaM from *E. coli* N5151 or AR68
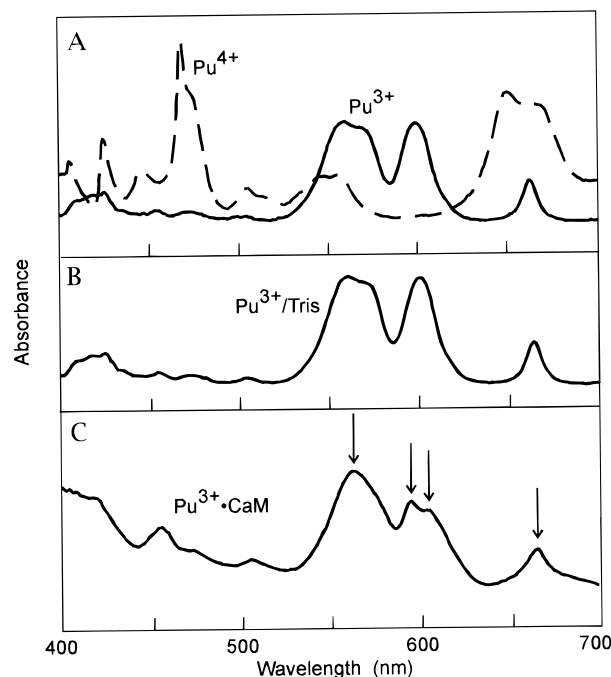

Figure 2. Plutonium solution absorbance spectra. (A) Pu^{4+} (dash line) and Pu^{3+} (solid line) in acid solutions (1 M HClO$_4$); (B) Pu^{3+} in 1 mM tris(hydroxylmethyl)aminomethane, pH 4.8 (the same spectra were obtained for pH 4.8$-$6.5); and (C) 4Pu^{3+}·CaM in 1 mM tris-(hydroxymethyl)aminomethane (500 mM KCl, pH $\sim$ 6.0).

containing the plasmid pCam23PL.[21] Purification was carried out as previously described.[11] (The first sample used for neutron measurements also included about 1/3 bovine CaM purchased from Calbiochem and used without further purification.) CaM was prepared for complexing with Pu^{3+} by first dialyzing against 50 mM tris(hydroxymethyl)aminomethane, 0.1 M KCl, and 2 mM EGTA (ethylene glycol bis(β-aminoethyl ether)-*N,N,N′,N′*-tetraacetic acid) at pH 7.0 to remove all the calcium, as well as other metal ions. Next it was dialyzed against 1 mM tris-(hydroxymethyl) aminomethane, 500 mM KCl, pH 6.0. Neutron-scattering samples were prepared in D$_2$O rather than H$_2$O in order to minimize the large incoherent neutron scattering from H. For the first neutron sample D$_2$O:H$_2$O exchange was achieved by repeated concentrations (4 times 40 mL to 10 mL) in an Amicon ultrafiltration device (YM5 filter). For the second neutron-scattering sample, dialysis was used instead of ultra-filtration to avoid protein loss through absorption on the membrane.

Preparation of the 4(^{240}Pu^{3+})·CaM Complex. Preparation of a Pu/CaM complex presents a number of challenges. Pu^{3+} has an ionic radius of 1.00 Å,[22] which is essentially the same as that of Ca^{2+}. Pu^{3+} would therefore be expected to bind readily to the Ca^{2+}-binding sites in CaM. Further, the greater ratio of charge-to-radius for Pu^{3+} is likely to give rise to tighter binding than is seen for Ca^{2+}. In order to make a Pu^{3+}/CaM complex, however, it is necessary to form a solution of Pu^{3+} in the pH range 5.5$-$6.0 since the protein will aggregate or precipitate at lower pH. This is a challenge because at pH higher than 4.0, Pu^{3+} oxidizes rapidly and forms an insoluble Pu^{4+} colloid. We approached this problem by trying to identify agents that would chelate Pu^{3+}, holding it in solution and inhibiting oxidation long enough to facilitate binding to CaM. The chelator also needed to be mild enough to release the Pu^{3+} to the CaM when needed. A variety of solutions were surveyed

(19) Debye, P. *Ann. Phys.* **1915**, *46*, 809$-$823.
(20) Newton, T. W.; Hobart, D. E.; Palmer, P. D. *Los Alamos National Laboratory Report, LA-UR-86-967*, 1986.

(21) Putkey, J. A.; Draetta, G. F.; Slaughter, G. R.; Klee, C. B.; Stull, J. T.; Means, A. R. *J. Biol. Chem.* **1986**, *261*, 9896$-$9903.
(22) Shannon, R. D. *Acta Crystallogr.* **1976**, *A32*, 751$-$767.

Table 1. Solution Conditions Tested for Stabilizing Pu^{3+} Near Neutral pH

solvent	pH	Pu^{3+} solubility
sodium Phosphate buffer (50 mM NaPO4, 100 mM KCl)	7.0	blue precipitate formed immediately
MOPS buffer (50 mM 3[*N*-morpholino]propanesulfonic acid, 100 mM KCl)	7.0	yellow precipitate formed immediately
sodium citrate buffer (50 mM $HOC(COONa)(CH_2COONa)_2$, 100 mM KCl)	6.0	complete oxidation to Pu^{4+} in 20 min
cacodylate buffer[a] (50 mM$(CH_3)_2AsO·OH$, 100 mM KCl)	6.5	20% of Pu^{3+} oxidized to Pu^{4+} in 1 h
ascorbate buffer (50 mM $C_5H_8O_6$)	4.0	Pu^{3+} stayed in solution[b]
(50 mM $C_5H_8O_6$)	4.5	Pu precipitated overnight
(50 mM $C_5H_8O_6$)	5.0	Pu precipitated overnight
(10 mM $C_5H_8O_6$, 100 mM KCl)	6.0	Pu precipitated overnight
Tris solutions[c] (10 mM tris(hydroxymethyl)aminomethane, 100 mM KCl)	6.5	Pu^{3+} stable 2−4 h
(10 mM tris(hydroxymethyl)aminomethane, 500 mM KCl)	6.0	Pu^{3+} stable 2−4 h
(1 mM tris(hydroxymethyl)aminomethane, 500 mM KCl)	6.0	Pu^{3+} stable 2−4 h

[a] CaM binding experiments with Pu in cacodylate buffers resulted in no Pu binding to the protein, possibly because the cacodylate chelated the Pu too tightly. [b] Low pH causes CaM to precipitate. [c] The Tris solutions were not buffers, and the pH drifted down to between 5 and 6 for these experiments.

for their ability to stabilize Pu^{3+} at pH 5.5−6.0, and the results are given in Table 1. KCl was used to keep the ionic strength of the solution in a range known to be favorable to keeping the protein in solution, free of aggregation and structurally stable. The Tris solutions used had very little buffering capacity, but were the most effective at keeping the Pu^{3+} in solution for long enough times to make the complexes with CaM. Thus to prepare Pu-complexed CaM, the $^{240}Pu^{3+}$ stock was diluted with 1 mM tris(hydroxymethyl)aminomethane (500 mM KCl, pH 6.0) in D_2O. A flat-bottomed glass tube that had been soaked in EDTA (ethylenediaminetetraacetic acid, to remove metal ions) and thoroughly rinsed was used to contain the solutions in the binding process. A small Teflon-coated stirbar provided rapid stirring to lessen local acid shock to the protein. The Pu^{3+} was added in 100-mL aliquots by placing the pipet tip near the stirbar and releasing the Pu^{3+} slowly. Sufficient Pu^{3+} was added to achieve a 4:1 Pu^{3+}:CaM stoichiometry, with no excess. Small amounts of CaM came out of solution but quickly redissolved. The final product was a clear blue solution characteristic of Pu^{3+}.

Absorbance spectra were used to characterize Pu and Pu/CaM complexes, as shown in Figure 2. The comparison of Pu^{3+} and Pu^{4+} in strong acid (Figure 2A) shows the characteristic differences between these species, and Figure 2B demonstrates the purity of Pu^{3+} in 1 mM tris(hydroxymethyl)aminomethane. On forming the complex with CaM, the Pu^{3+} spectrum (Figure 2C) remains Pu^{3+}-like, with some perturbations. The broad double peak around 560 nm becomes a narrower single peak. The single peak at 600 nm splits into two features at 597 and 603 nm, while the sharper peak at 662 nm is relatively unchanged. The Pu^{3+}·CaM spectrum also shows a rising background with increasing intensity toward shorter wavelengths, due to the protein absorbing strongly in the UV. A titration experiment was done adding mole equivalents of Pu^{3+} sequentially to CaM, and the intensity of the Pu^{3+} peaks in the spectrum was plotted (Figure 3). The spectral peaks at 502, 597, and 603 nm show a distinctive linear increase in intensity with 1 through 4 mol equiv of Pu^{3+} added, and then a flat plateau. The peak at 662 nm which was unperturbed by complexing Pu^{3+} with CaM increases linearly for 1 through 6 mol equiv added. These results indicate that there are indeed four specific Pu^{3+}-binding sites in CaM.
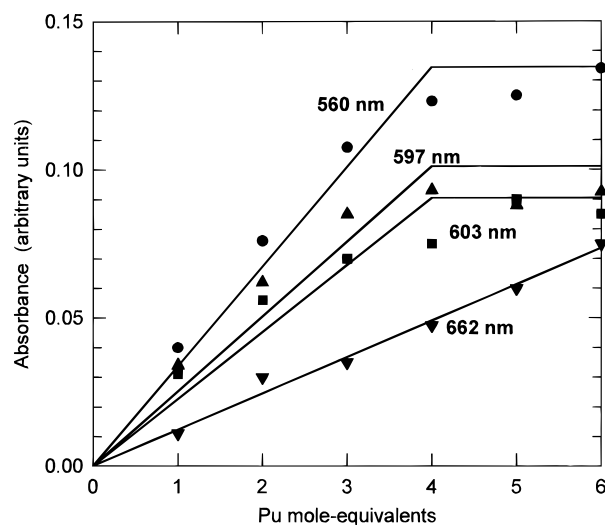

Figure 3. Absorbance intensities from the Pu^{3+}/CaM complex as a function of mole equivalents of addition of Pu^{3+}. Several of the features show a linear increase between 0 and 4 mol equiv of Pu^{3+}, followed by a flattening. This indicates that there are four binding sites for Pu^{3+} in CaM.

Neutron-scattering data were collected from samples of $4(^{240}Pu^{3+})$·CaM made in two independent preparations. The calculated protein concentrations for the two samples were 50 and 44 mg/mL, prepared for the first and second neutron experiments, respectively. The freshly prepared samples for neutron scattering were transferred into a quartz cell 27 mm wide by 28 mm high by 4 mm thick, for a total volume of 3 cm^3. This cell was in turn encapsulated in a secondary containment vessel with quartz windows and a boron nitride (BN) mask to define the exposed area. The calculated CaM molecular area densities were 0.72×10^{18} and 0.63×10^{18} cm^{-2}. Over the period of the neutron-scattering experiments (several days), some of the initial characteristic Pu^{3+} blue color faded indicating some oxidation of the Pu^{3+}. Since there was no accompanying evidence of Pu^{4+} colloid formation and precipitation, we assume the oxidized Pu remained bound to the protein. This conclusion is supported by the fact that the neutron resonance scattering

yielded the characteristic distance separation expected for the bound Pu.

Neutron-Scattering Data Acquisition. Two independent sets of neutron measurements were made on the Low-Q Diffractometer (LQD) at the MLNSC on the two independent sample preparations. To optimize for short-wavelength neutrons, three changes were made to the usual operational procedures of LQD.[23] First, the single-crystal MgO filter normally used to remove short-wavelength neutrons was rotated out of the beam. The time-of-flight range in the software was adjusted to begin at an earlier time (corresponding to 0.243-Å neutrons) and the time resolution was set to $\delta t/t = 0.5\%$. Finally, the multi-aperture collimation system with five separate beams was used;[24] this improves angular resolution by using smaller apertures, but simultaneously increases count rate by using larger areas of the moderator and sample. All of these changes required a recalibration of the instrument. It had previously been determined that one of the five aperture sets could not be aligned to the same point on the detector, and hence had to be blocked with a mask of ^{6}LiF. Short runs were also made with the "normal" LQD configuration to measure the radius of gyration, R_g, of the 4Pu^{3+}·CaM.

In the first neutron experiment, the 4(^{240}Pu^{3+})·CaM sample was run for a total of 15.7 beam hours with an average proton beam current on the neutron-producing target of 60 μA. An identical cell containing only the Tris/KCl/D$_2$O solvent was measured for 7.4 h at an average current 64 μA. For each case the sample transmission was measured by attenuating the beam with 6.3 mm of BN and removing the beamstop from in front of the detector for about 30 min. All runs were normalized to integrated counts of the beam-current signal provided by the facility. A short "blocked beam" run was also made, using the same BN attenuator and with the beamstop in place. In retrospect it was found that this signal was not useful in determining non-beam-related background because the transmission of the BN near 0.278 Å was too large; lack of this information meant that interpretation of the transmission data was difficult, and only qualitative analysis of the data was possible following the first experiment.

For the second neutron experiment the liquid hydrogen moderator normally serving LQD was replaced with an ambient temperature water moderator which provided a spectrum of neutrons that should have better favored the ^{240}Pu resonance experiment (providing greater flux at 0.278 Å). In addition, a beam-monitoring detector was installed in the beamstop, allowing an independent direct measurement of the transmitted flux during the experiment.[25] The second 4(^{240}Pu^{3+})·CaM sample was run for 28.3 h at 68 μA, and the solvent was run for 19.9 h at 74 μA. These runs were normalized by the respective transmitted beam monitor counts. The blocked beam run was made by using a thickness of 15.4 mm of BN with a transmission less than 10^{-4} at the resonant wavelength for 6.8 h at 77 μA. The background measurement and the transmission measurements from the second run made it possible to extract quantitative information from the first data set. Both sets of neutron data showed evidence for the same periodic term in the resonance-scattering term. Shown here is the analysis of the first data run, which had a flatter non-resonant-scattering term, possibly due to the lower background scattering from the liquid hydrogen moderator.
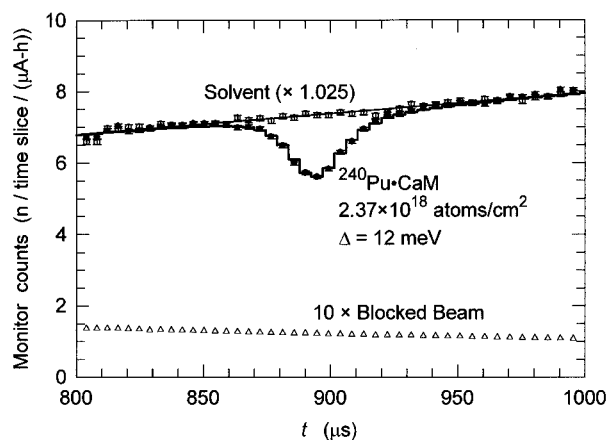

Figure 4. Measured ^{240}Pu transmission from the second neutron-scattering experiment. The histogram is a theoretical calculation with two free parameters.

Since the LQD is on a pulsed source, neutron time of flight is used to measure the velocity (and hence wavelength) of each neutron. The flight time is measured from the instant at which protons strike the spallation target, producing the neutron pulse, and is about 900 μs at the resonant wavelength. All data were collected as 3-dimensional (X, Y, t) histograms of counts per 3.4×3.4 mm^2 detector pixel and per 0.5% time slice. Only 24 of the time slices (wavelengths of 0.261$-$0.295 Å) were used directly for resonance analysis.

Neutron-Scattering Data Reduction and Analysis. The process of data reduction is to use the signal and transmission histograms, normalized and corrected for efficiencies and various forms of backgrounds, to obtain $I(Q)$ and eventually $F_{rr}(Q)$, the form factor for the separations of the ^{240}Pu atoms. The first stage was to analyze the long-wavelength data to see if the overall solution conformation of 4Pu^{3+}·CaM is the same as 4Ca^{2+}·CaM. The probable frequency distribution of interatomic vectors ($P(r)$, calculated as the inverse Fourier transform of $I(Q)$) for the Pu-complexed CaM showed the same general features as that previously published for 4Ca^{2+}·CaM[6], i.e. a peak at $\sim$18 Å, with a shoulder at $\sim$45 Å, and a maximum linear dimension of $\sim$65 Å, indicating the overall dumbbell shape of the protein is preserved. The radius of gyration derived from the second moment of $P(r)$ is $R_g = 22.3 \pm 0.2$ Å, which is $\sim$5% larger than the previously measured value for 4Ca^{2+}·CaM in D$_2$O solution, 21.3 ± 0.2 Å[6]. This small difference could reflect differences in the Pu^{3+} vs Ca^{2+} induced conformational changes within the individual globular domains of the protein. It is known that metal binding to CaM results in a "hinge" opening within each globular domain. Indeed such hinge opening is observed upon Ca^{2+} binding,[26-28] resulting in a 9% increase in R_g while preserving the overall dumbbell conformation of the protein.[6] The different charge-to-radius ratios for the Ca^{2+} and Pu$^{3+/4+}$ ions might be expected to result in different degrees of hinge opening.

The sample transmission as measured by a ^{6}LiF glass scintillation detector mounted in the beamstop[25] is illustrated for the second neutron-scattering measurement in Figure 4. The blocked-beam signal (which has been subtracted from both data sets) is not a significant term for this detector. The solvent signal was normalized at 80$-$100 μs on either side of the

(23) Seeger, P. A.; Hjelm, R. J. P. *J. Appl. Crystallogr.* **1991**, *24*, 467$-$478.

(24) Seeger, P. A. *Physica (Utrecht)* **1986**, *136B*, 106$-$109.

(25) Seeger, P. A.; Hjelm, R. J. P; Nutter, M. J. *Mol. Cryst. Liq. Cryst.* **1990**, *180A*, 101$-$117.

(26) Zhang, M.; Tanaka, T.; Ikura, M. *Nature Struct. Biol.* **1995**, *2*, 758$-$767.

(27) Kuboniwa, H.; Tjandra, N.; Grzesiek, S.; Ren, H.; Klee, C. B.; Bax, A. *Nature Struct. Biol.* **1995**, *2*, 768$-$776.

(28) Finn, B. E.; Evenäs, J.; Drakenberg, T.; Waltho, J. p.; Thulin, E.; Forsén, S. *Nature Struct. Biol.* **1995**, *2*, 777$-$783.

resonance of the $4(^{240}\mathrm{Pu}^{3+})\cdot$CaM signal (a correction of 2.5% from the beam current monitor signal) and then fitted with a straight line in the vicinity of the resonance. The theoretical ^{240}Pu cross section must be convoluted with Doppler broadening and with the instrument time-of-flight resolution, which has terms due to the width of the recorded time slice (4.47 μs), the proton pulse width (0.27 μs), and the pulse shape distribution of the moderator. This last function has been calculated by a detailed Monte Carlo simulation of the MLNSC target/moderator system[29,30] and is very well fitted near the resonance wavelength by an Ikeda−Carpenter function,[31] $(t/\lambda)^2 e^{-(0.257 t/\lambda)}$, with 70% of the neutrons emitted directly and 30% convoluted with an exponential decay, $e^{-(t/6.8)}$ (for t in μs and λ in Å). Doppler broadening[32] results from thermal motion of the ^{240}Pu nuclei. The velocities of the CaM molecules are small compared to the neutron velocity, but the ^{240}Pu atoms are vibrating within their CaM binding sites. If we neglect Doppler broadening, the resulting computed resolution is too narrow, and if we use the value of the mean-square velocity appropriate for metallic Pu as in ref 32, it is too broad. We have therefore taken the thermal width to be a free parameter and have chosen 12 meV as the best fit. Since the resolution is asymmetric and the transmission is nonlinear, Monte Carlo is the best technique for applying both the Doppler and the resolution corrections. A program using library MCLIB[33] determined the number of counts per time slice, averaged over all wavelengths which may contribute to the slice, as a function of the density of ^{240}Pu atoms. The histogram line in Figure 4 is thus a theoretical curve, with density and Doppler width as the two free parameters. The area density of ^{240}Pu atoms was found by iteration, giving 2.37 $\times$ 10^{18} atoms/cm^2, which is 6% lower than 4 times the estimated CaM density; this is partly because the sample did not completely cover the exposed area of the cell, but may also represent some small deterioration of the sample.

The histogram in Figure 4 shows that the wavelength calibration is excellent and the shape of the resonance is very well understood. We can therefore use this measurement, corrected for the different ^{240}Pu density, in the reduction of the first neutron data set. Also, the Monte Carlo procedure provides independent averages of $\lambda(t)$ and its standard deviation, Re$\{b(t)\}$, Im$\{b(t)\}$, and $|b(t)|$ appropriately weighted by resolution and transmission probability. These averages depend on the ^{240}Pu density; *e.g.*, the peak value of $|b|$ is reduced because fewer neutrons are transmitted at the peak. The terms needed for the decomposition of eq 5 are shown for the first neutron sample density in Figure 5, which may be compared to Figure 1A. The wavelength resolution (rms), including the width of the recorded slices, is 0.63%.

The usual normalization and background subtraction for LQD data is to divide the recorded histogram for the signal, (S), by the transmitted beam, (T_S), and subtract the buffer, (B), divided by its transmitted beam, (T_B). If, however, there is a significant difference in the two transmission functions, and if there is also a significant background that is sample independent, then an additional correction term is necessary. Let (K) represent a

(29) Pitcher, E. J.; Russell, G. J.; Seeger, P. A.; Fergusson, P. D. *ICANS-XIII*; Paul Scherrer Institut: Villigen, Switzerland, Oct 11−14, 1995; PSI Proceedings 95−02, pp 323−329.

(30) P. D. Fergusson provided Monte-Carlo calculations of the performance of the as-built MLNSC target-moderator system.

(31) Ikeda, S.; Carpenter, J. M. *Nucl. Instrum. Methods* **1985**, *A239*, 536−544.

(32) Seeger, P. A.; Taylor, A. D.; Brugger, R. M. *Nucl. Instrum. Methods* **1985**, *A240*, 98−114.

(33) Seeger, P. A. *ICANS-XIII*, Paul Scherrer Institut: Villigen, Switzerland, Oct 11−14, 1995; PSI Proceedings 95-02, 323−329. The Monte Carlo program referenced here and its description are available by anonymous ftp from *azoth.lansce.lanl.gov/pub/mclib*.
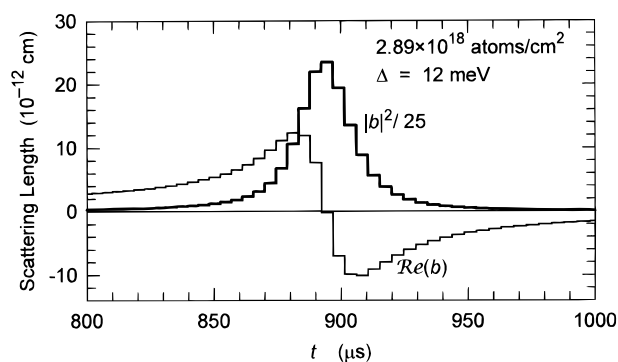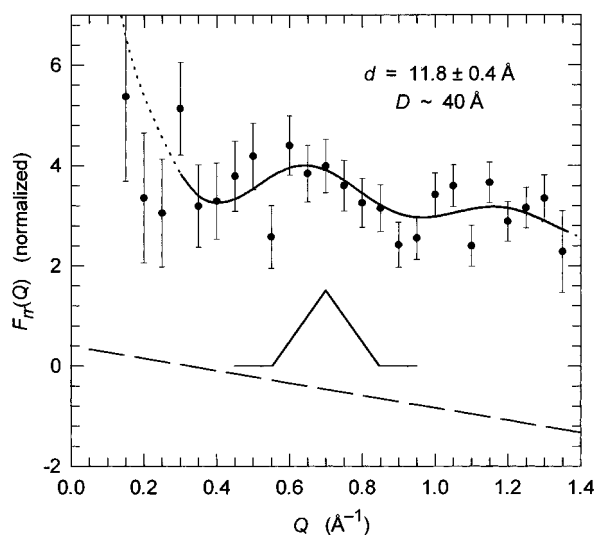

Figure 5. Weighted averages of resonant scattering length, including effects of the asymmetric neutron pulse shape, resonant absorption, and Doppler broadening for the first neutron-scattering experiment.

blocked-beam measurement, and suppose the relative normalization factors of the three measurements are N_S, N_B, and N_K. Then we can subtract the blocked-beam component of the signals before normalizing the transmitted beams as

$$I = \frac{(S) - (K)N_S/N_K}{(T_S)} - \frac{(B) - (K)N_B/N_K}{(T_B)}$$

$$= \frac{(S)}{(T_S)} - \frac{(B)}{(T_B)} - \frac{(K)}{N_K}\left[\frac{N_S}{(T_S)} - \frac{N_B}{(T_B)}\right] \qquad (7)$$

The second form is preferred because it allows propagation of errors without correlations, and also shows (K) as a correction to the standard form. Since $(T_S)/N_S$ and $(T_B)/N_B$ are exactly the functions which were fitted in the construction of Figure 4, the coefficient of (K) can be computed precisely. To minimize the statistical uncertainties in the transmission measurements the measured (T_B) was fitted over the relevant time range with a second-order curve and (T_S) was computed by multiplying by the transmission curve corresponding to Figure 5. The blocked-beam correction was a major fraction of the signal and contributed to the statistical uncertainty of the data points; it did not, however, affect the final result.

For each of 24 time slices around the resonance, the detector (X, Y, t) histogram was binned in a uniform Q-scale. For each value of Q the three orthogonal form factor terms of eq 5 were then extracted by least squares. Correlations of the errors with the small F_{00} and F_{0r} terms prevent assignment of simple error bars to F_{rr} obtained in this extraction. Therefore simple expressions for F_{00} and F_{0r} as a function of Q were subtracted from the data and F_{rr} was extracted again. The error bars could then be propagated from the counting statistics (see Figure 6). In this process all of the errors are assigned to F_{rr}. Systematic bias may occur in the processes of dividing by the computed transmission and normalizing the background and blocked-beam subtractions. The dashed line on Figure 6 is a linear correction computed in the model-fitting process. The resolution in Q is dominated by the size and shape of the neutron beam spot, which is a triangular distribution with a measured full width half maximum of 28 mm. The resulting Q resolution, with full width half maximum = 0.15 Å^{-1}, is illustrated in Figure 6.

If we assume the CaM molecules are non-interacting, then the range of the double sum of eq 6 is just the four binding sites within the molecule, a total of sixteen terms. We further simplify by assuming the distances between the two sites within each globular domain are equal, d, based on the knowledge that the domains are structurally homologous (the crystal structure of 4Ca$^{2+}\cdot$CaM shows the separations of Ca^{2+} ions within each globular domain to be 11.85 and 11.49 Å which are equal within

Figure 6. Resonant scattering form factor, F_{rr}, calculated for the scattering data from the first neutron experiment. Error bars are propagated from counting statistics; data-reduction procedures were chosen to minimize correlations between points. Systematic bias estimated from the least-squares model fit is indicated by the dashed straight line. The triangular distribution is the instrumental (angular) resolution. The resulting smeared model fit is the solid curve.

the precision of our measurements). We also assume the four distances between sites in opposite domains may be represented by an average, D. The resulting model is

$$F_{rr}(Q) = 4 + 4 \sin(Qd)/Qd + 8 \sin(QD)/QD \qquad (8)$$

More generally, D may be replaced by a probability density and the final term by an integral over the range of D. Reasonable values for the range of D, from the crystal structures of extended and of collapsed configurations of CaM,[34,9] would be from about 31−48 Å, with the average of the four distinct distances being 45.8 and 36.1 Å for the two configurations respectively.

Before fitting to the experimental data, the model must be "smeared" by the instrumental resolution; this was accomplished by a (triangular) weighted sum of eq 8 evaluated at 11 points in the range $Q \pm 0.15$ Å^{-1}. Weighted nonlinear regression was performed in SigmaPlot,[35] which uses the Marquardt−Levenberg algorithm. Although a precise and robust value of d was found, the program was unable to solve for D. Constraining D to fixed values in the range 20−60 Å, the fit improves very slightly up to $D = 40$ Å and is identical for all higher values. This is because whenever the full width of the resolution function covers more than two oscillations of the function, *i.e.*, for $D > 2\pi/0.15 = 43$ Å, all information has been completely lost. Since we begin to lose sensitivity at half this value, $D > 22$ Å, the experiment did not provide any direct information on D in the range of interest. A value must be included for D, however, to give the rise of the data at low Q. The curve through the data in Figure 6 is the fitted result:

$$d = 11.8 \pm 0.4 \text{ Å}$$

with D set to $\sim$40 Å. This value for d is robust in the sense that it does not depend strongly on the resolution function. For instance, if Doppler broadening is neglected the value d changes

(34) Babu, Y. S.; Bugg, C. E.; Cook, W. J. *J. Mol. Biol.* **1988**, *204*, 191−204.

(35) Jandel Corporation. *SigmaPlot for Windows*, Version 3.0, 1995.

by less than 1%, and if the blocked-beam correction is reduced by 50%, d becomes 11.6 Å.

Discussion and Conclusions

In the experiments reported here we were successful in identifying conditions whereby Pu^{3+} is stable in near neutral pH solutions for 6−7 h. Tris(hydroxymethyl)aminomethane was shown to chelate Pu^{3+} sufficiently strongly to keep it from oxidizing and precipitating over this time period, but the chelation was also weak enough so that addition of CaM to the Pu^{3+}/Tris solution resulted in the release of the Pu^{3+} from the tris(hydroxythmethyl)aminomethane and its binding to CaM. The Pu/CaM titration data combined with the distance measurement from the neutron resonance scattering demonstrate that the Pu binds specifically to the four Ca^{2+}-binding sites in CaM. This is the first demonstration of binding of Pu to specific sites in a protein. We have also demonstrated that interatomic distances of specific sites in macromolecules in solution may be determined with a precision of 3% by small-angle neutron scattering, by substitution of nuclei with strong nuclear resonances, especially ^{240}Pu. The value of 11.8 ± 0.4 Å obtained for the average distance between the two Ca^{2+}-binding sites in the same globular domain of CaM agrees with the crystallographic average of 11.7 Å.[34] Thus the measurement is both precise and accurate. The precision of our measurement based on data of relatively poor statistical quality (Figure 6) results from using the detailed shape of the nuclear resonance to select neutron wavelengths and fitting the model parameter over a relatively wide Q range. The dynamic range of the experiment was limited by the angular resolution of the small-angle instrument collimation to distances of about 7−30 Å. Future spallation neutron sources, now in design stages, will have the much higher intensity required to support instruments with higher angular resolution which will extend the available range to both higher and lower values. Such sources will also make it possible to do experiments with smaller samples and lower concentrations, and/or with higher precision. Further, they will facilitate use of other resonance scatterers (see the list in the Introduction) that may have less "ideal" resonant properties compared with ^{240}Pu, but are easier to work with. Collimation systems and detector shielding of future instruments must be designed to minimize the "blocked-beam" contribution to the background, which made a major contribution to the statistics of the data in this experiment.

The specific binding of Pu^{3+} to the Ca^{2+}-binding sites of a key regulatory protein leads one to speculate on possible mechanisms for health effects from Pu. Biochemical regulation is critical to healthy function, and breakdown of regulation leads to uncontrolled cell growth and proliferation and, if not corrected, cell death. Nature regulates biochemical activity through the use of a number of "messengers", among which the divalent calcium ion is perhaps the simplest and most widespread. Ca^{2+}-dependent regulation generally involves equilibrium binding to a receptor protein. The kinetics of the "on" and "off" rate constants for the Ca^{2+} binding are delicately balanced so that when there is a particular extracellular stimulus, an increase in local Ca^{2+} concentrations within a cell is effected, which in turn results in Ca^{2+} binding to specific proteins that eventually cause specific pathways to be switched "on". A pathway is switched "off" again when the local Ca^{2+} concentration drops. Many Ca^{2+}-binding regulatory proteins have Ca^{2+}-binding sites that strongly resemble those in CaM. The fact that the 4Pu·CaM samples were stable for several days suggests the Pu^{3+} binding is very tight, consistent with our expectation based on its higher charge-to-radius ratio compared with Ca^{2+}.

Other ionic species of Pu, including the more stable Pu^{4+}, might bind even more tightly; thus even at low Pu concentrations there could be permanent binding to Ca^{2+} regulatory sites resulting in complete disruption of the normal kinetics. One is tempted, therefore, to speculate that Pu binding to regulatory proteins could be a factor in breakdown of cellular regulation and subsequent expression of toxic effects, or even neoplastic transformation of a cell. Such mechanisms of metal toxicity have been discussed.[15,16] Binding to Ca^{2+} regulatory sites could also provide a means by which Pu is transported directly to DNA-containing sites in cells, thus facilitating radioactive damage to DNA.

JA9633124